NATIONAL AERONAUTICS AND SPACE ADMINISTRATION

Technical Memorandum 33-643

Experimental Evaluation of Fluctuating Density and Radiated Noise From a High-Temperature Jet

P. F. Massier

S. P. Parthasarathy

R. F. Cuffel

JET PROPULSION LABORATORY

CALIFORNIA INSTITUTE OF TECHNOLOGY

PASADENA, CALIFORNIA

October 1, 1973

NATIONAL AERONAUTICS AND SPACE ADMINISTRATION

Technical Memorandum 33-643

Experimental Evaluation of Fluctuating Density and Radiated Noise From a High-Temperature Jet

P. F. Massier
S. P. Parthasarathy
R. F. Cuffel

JET PROPULSION LABORATORY
CALIFORNIA INSTITUTE OF TECHNOLOGY
PASADENA, CALIFORNIA

October 1, 1973

Prepared Under Contract No. NAS 7-100
National Aeronautics and Space Administration

PREFACE

The work described in this report was performed by the Propulsion Division of the Jet Propulsion Laboratory.

ACKNOWLEDGMENT

This report was presented at the Advisory Group for Aerospace Research and Development (AGARD), Fluid Dynamics Panel Meeting, Brussels, Belgium, September 19 - 21, 1973.

CONTENTS

FIGURES

CONTENTS (contd)

FIGURES (contd)

TABLE

APPENDIX

FIGURES

ABSTRACT

An experimental investigation has been conducted to characterize the fluctuating density within a high-temperature (1100 K) subsonic jet and to characterize the noise radiated to the surroundings. Cross correlations obtained by introducing time delay to the signals detected from spatially separated crossed laser beams set up as a Schlieren system were used to determine radial and axial distributions of the convection velocity of the moving noise sources (eddies). In addition, the autocorrelation of the fluctuating density was evaluated in the moving frame of reference of the eddies. Also, the autocorrelation of the radiated noise in the moving reference frame was evaluated from cross correlations by introducing time delay to the signals detected by spatially separated pairs of microphones. The radiated noise results are compared with Lighthill's theory and with the data of Lush. Radial distributions of the mean velocity were obtained from measurements of the stagnation temperature, and stagnation and static pressures with the use of probes.

1. INTRODUCTION

Perhaps the most significant obstacle to the full understanding of the noise sources in free jet flows is the formidable task of experimentally characterizing the turbulence generated in the shear region. A complete experimental evaluation of the distribution of fluctuating quantities (or noise sources) within jets and the determination of the contribution of each source to the noise radiated at a particular location outside the jet appears at present to be almost unobtainable in a practical sense. This is true even with the use of recently developed instrumentation methods coupled with the use of high-speed computers for data analysis purposes. Thus, any investigation of the fluctuating quantities related to the radiated noise requires simplifications in terms of a model that "represents" the real situation.

The experimental investigation to be discussed pertains to one method of characterizing the fluctuating quantities that generate the noise as well as to a method of characterizing the noise that is radiated to the surroundings. In particular, the fluctuating densities in a high-temperature subsonic jet have been characterized by the use of cross correlations that were obtained by introducing time delay to the signals detected from spatially separated crossed laser beams that were projected through the jet. The lasers were set up as a Schlieren system. From the cross correlations of the spatially separated beams the convection velocity of the moving eddies and the fluctuating density autocorrelations were evaluated. Conceptually the eddies consist of statistically random fluctuations in density that can be identified as they move along the flow direction. These eddies are considered to be the noise sources. The density autocorrelation is the envelope of a family of the cross correlation curves. This autocorrelation function is the intensity of the density fluctuations ($2\overline{\rho_H' \rho_V'}$) in the moving frame of reference of the eddies, or also; it is the Fourier transform of the fluctuating density spectrum.

Simplifications introduced into the data analysis procedure include the assumptions of isotropy and homogeneity; however, a method of treating nonisotropic fluctuations is discussed. Then, even though radial as well as axial distributions of the intensity of the density fluctuations and of the convection velocity were obtained, the characterization is based on a model consisting of point noise sources concentrated along the axis of the jet; consequently, it was assumed that the noise was essentially being radiated from a line antenna.

A distinct advantage in an experimental sense of dealing with the fluctuating density rather than with the fluctuating pressure is that the density and the two-point correlations can be evaluated comparatively easily without disturbing the flow. Such disturbances could occur, for example, with the use of probes, particularly since two probes close to each other would be required in order to obtain two-point correlations.

The radiated noise is compared with the theory of Lighthill (Ref. 1) and with some of the data obtained by Lush (Ref. 2). In addition, it is characterized in terms of the noise cross-correlation coefficient and the autocorrelation function in the moving frame of reference of the eddies. Correlations of the radiated noise were evaluated from the signals obtained with pairs of microphones by introducing time delay.

The experiments were conducted in an anechoic chamber. The jet flow emerged from a convergent-divergent nozzle in which flow separation occurred downstream of the throat because the nozzle was considerably overexpanded. Consequently, a shock structure was established but was contained entirely within the nozzle and the flow was subsonic and shock-free at the nozzle exit as verified by Schlieren and shadowgraph observations. The average stagnation temperature at the nozzle inlet taking into account all tests was about 1100°K (1520°F) and the Mach number at the nozzle exit was about 0.5. Radial distributions of mean values of the velocity, stagnation temperature, stagnation pressure and static pressure were obtained in the jet with the use of probes.

2. CONVERSION OF LIGHTHILL'S THEORY TO THE POINT SOURCES

The theoretical work of Lighthill (Refs. 1 and 3) is based on the concept of quadrupole sources distributed over the volume of the jet. The analysis of the experimental data to be discussed, however, is based on the model of point noise sources concentrated along the axis of the jet. Measurements were made throughout the jet region with the laser beams to obtain radial and axial distributions of the fluctuating density; however, the amount of such mapping is far from adequate for direct use in Lighthill's theory. Nevertheless, it is possible to demonstrate that the Lighthill theory can be converted into a form which for quadrupole sources resembles the autocorrelation function derived directly from the point-source model. The analysis of this conversion is omitted for brevity; however, the procedure followed includes (1) integration of the cross correlation function over a noise source (or eddy), (2) integration over the cross section of the jet, and (3) conversion of the integral along the axis to an integration of the emission time. The emission time is the time interval required for the noise to propagate from a source to a microphone. During this time interval the noise source will have traveled to a new location. The final expression for the correlation function is

$$C(\tau) = \frac{1}{16\pi^2} \int \frac{[2 \sin\theta_1 \cos\theta_1][2 \sin\theta_2 \cos\theta_2]}{r_1[1 - M_c \cos\theta_1]^2 \, r_2[1 - M_c \cos\theta_2]^3} \Psi_q \left(x - a_o M_c [0 - t_e], \, t_e; \, t^* - 0 + \frac{r_1}{a_o}\frac{r_2}{a_o} \right) dt \quad (1)$$

Equation (1) corresponds to the point-source model, Eq. (A3-1) of Appendix A3. It should be noted that in Eq. (A3-1) the factor $1/16\,\pi^2$ has been included in the definition of the source strength and as a consequence is contained in the noise autocorrelation function Ψ_n. The trigonometric terms in the numerator of Eq. (1) result from the definition of the quadrupole as does the quantity $[1 - M_c \cos\theta_2]$ being a cubed term instead of a squared term. Ψ_q in Eq. (1) is the autocorrelation function of a quadrupole in the moving frame of reference of the eddies. Its functional relationship is similar to that of Ψ_n of Eq. (A3-1). The two equations are identical in content.

3. EXPERIMENTAL FACILITY

The experiments were conducted in an anechoic chamber which is described in Ref. 4. During these experiments air from the outside was drawn into the chamber by the small decrease in ambient pressure inside, which was caused by the injector action of the jet. Before entering the chamber the outside air was distributed behind the wedge blocks that lined the room, and then the air entered through small spaces between the wedges as shown in Fig. 1. This minimized the possibility that significant recirculating flow patterns would occur inside the chamber.

Compressed air was supplied on a steady state basis by a compressor plant facility and was heated using a turbojet burner. The burner was located a considerable distance (227 cm) upstream of the nozzle so that good mixing of the flow could occur before it entered the nozzle. The diameter of the duct located between the burner and the nozzle was 30.5 cm. The nozzle throat diameter was 4.1 cm; thus the contraction area ratio was large with low velocities upstream of the nozzle.

The noise produced by the upstream configuration was evaluated from measurements obtained with a 19 mm diameter dynamic microphone probe which was inserted on the centerline inside the large duct at a distance of 70 cm upstream of the nozzle exit plane. The probe had a nose cone and sensed the static pressure fluctuations. These tests were conducted under cold flow (ambient temperature) conditions over a range of stagnation pressures including the pressure at which the hot flow tests were made. The upstream noise inside the duct was predominantly a pure tone at 560 Hz; however, pure tones were not observed outside the jet under hot flow conditions. Hence, the noise generated in the flow upstream of the nozzle was not considered to be a significant contribution to the noise radiated from the jet.

4. INSTRUMENTATION

The noise radiated from the jet was measured with 3 mm and 6 mm dia. B&K microphones. They were placed in the vertical position such that the tips were on a horizontal plane passing through the centerline

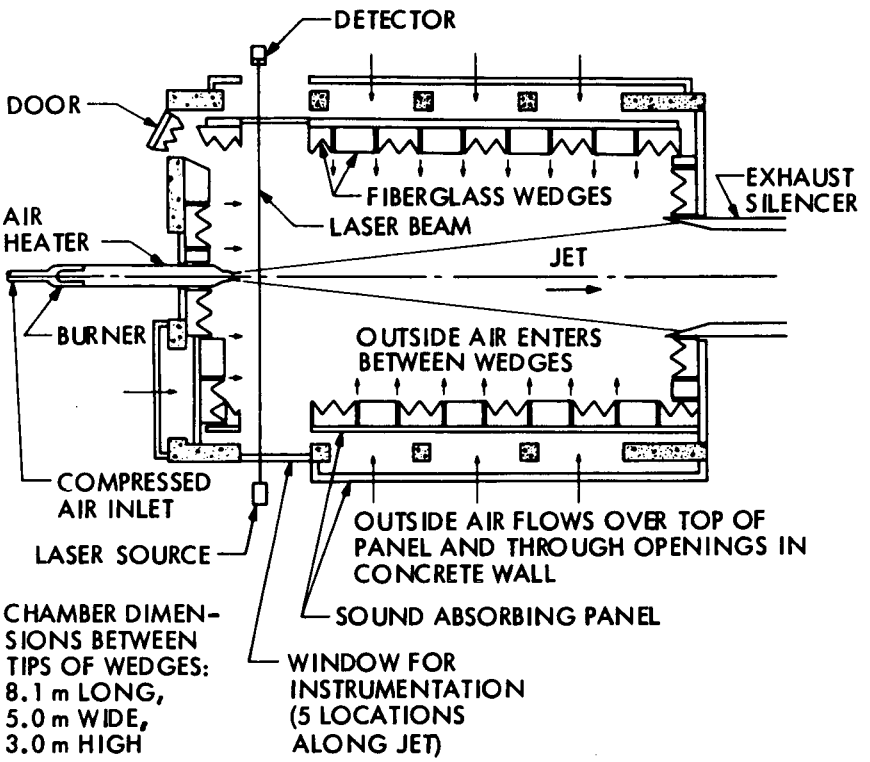

Figure 1. Anechoic Chamber Test Facility

of the jet. Hence, the sound waves grazed over the surfaces of the sensing elements. Eight microphones were located in a 60 cm diameter circle outside the jet stream. A diagram of the arrangement is shown in Fig. 2. The detected noise signals were recorded on magnetic tape and played back through a correlation instrument to obtain cross correlations. The procedure used to analyze the noise signals is discussed in Appendix A3.

Crossed laser beams from helium-neon sources were set up as a Schlieren system and projected through the jet as shown in Fig. 2. The beams, about 3 mm in diameter, were deflected by gradients in the refractive index which is related to the density by the Gladstone-Dale constant. Hence, fluctuations in density could be obtained from signals detected by the crossed-beam Schlieren arrangement. One beam was vertical and five additional beams, which were horizontal, were separated spatially across the diameter of the jet. Horizontal separation along the flow direction was obtained by moving the lasers to different locations during an experiment. Thus the jet could be scanned in both directions. The vertical beam could also be moved in either of two directions by adjusting a series of mirrors. Alignment of the knife edges of the Schlieren system and the reasons for the chosen alignment is discussed in Appendix A2. The detected laser signals were recorded on magnetic tape and then played back through a correlation instrument to obtain the cross correlations in the same manner as the noise signals. The analysis that was used to interpret the laser signals is discussed in Appendix A2 also.

Radial distributions of the mean jet velocity were determined from pitot pressure, static pressure, and from stagnation temperature measurements across the flow. Manometers were used to measure the pressures and shielded thermocouples were used to determine temperatures. Numerous probes mounted in line were used to obtain these pressures and temperatures.

The stagnation pressure at the nozzle inlet was measured with a pitot probe and the stagnation temperature at this location was obtained with a thermocouple probe.

Both Schlieren (in addition to the laser system) and shadowgraph systems were used to observe the flow patterns within the jet.

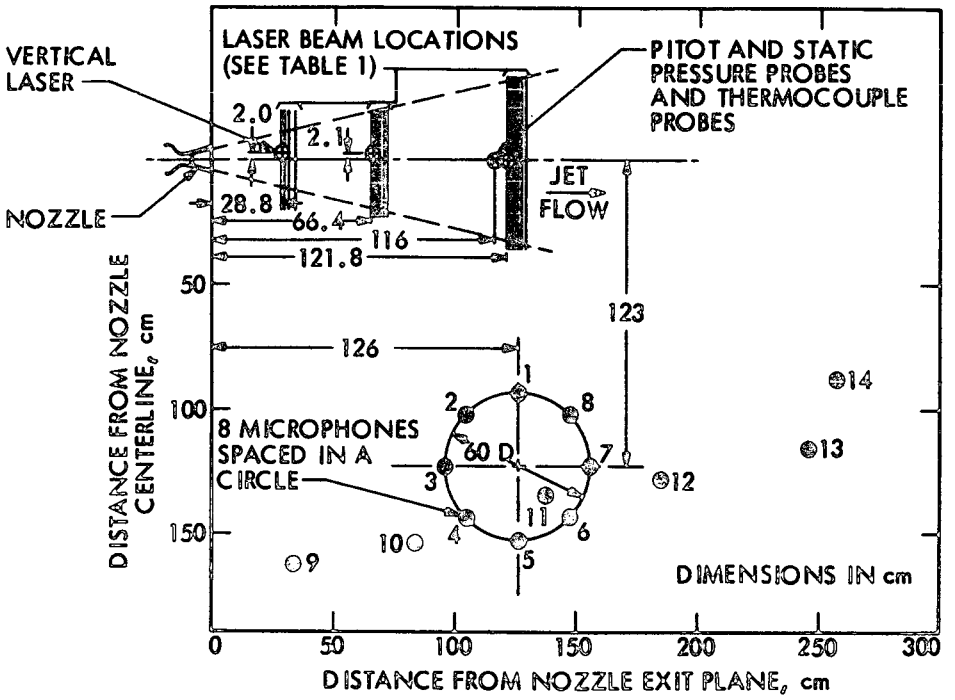

Figure 2. Instrumentation Locations

5. NOZZLE FLOW FIELD

The jet flow discharging from the nozzle exit plane was subsonic; however, for a portion of the distance downstream of the throat within the nozzle the flow was supersonic. Consequently, a discussion of the flow field inside the nozzle is needed to clarify this transition.

At the nozzle inlet the stagnation temperature averaged over numerous tests was 1100°K (1520°F) and the average stagnation pressure was 3.48 bar (50.4 psia). The variation in temperature was not more than ± 15°K and the variation in pressure was not more than ± 0.024 bar. The flow discharged into air at virtually atmospheric conditions inside the anechoic chamber from a convergent-divergent nozzle which was considerably overexpanded. The measured pressure inside the anechoic chamber was only 0.006 bar less than atmospheric pressure. Flow separation occurred inside the nozzle in the divergent section downstream of the throat as indicated by the pressure rise shown below the sketch of the nozzle in Fig. 3. At the flow separation location the Mach No. near the wall was 2.2 An oblique shock wave associated with the separation was established near the wall of the nozzle as shown in the figure. This wave projected downstream and intersected with a normal shock (shock stem or Mach disk) which crossed the centerline. The reflected oblique wave which projected downstream of this wave intersection was then reflected again from the separated flow region. This second reflection was deduced from a second rise in the wall static pressure as indicated in Fig. 3. Separated flow near the wall occurred between the two oblique waves as well as downstream of the second oblique wave. This was concluded from the observed constant wall pressures in these two regions even though the pressure levels differed.

The measurements that were made to locate these waves consisted of (1) wall pressures from which the flow separation and the angles of both of the oblique waves were determined, and (2) pitot probe pressure measurements along the centerline in a cold jet from which the existance and location of a normal shock wave which crossed the axis was established. These waves were probably curved, rather than being straight as shown. Their actual shapes are not known because the extent of the measurements was too limited. Additional discussion of these waves and the corresponding flow field may be found in Ref. 5. In addition,

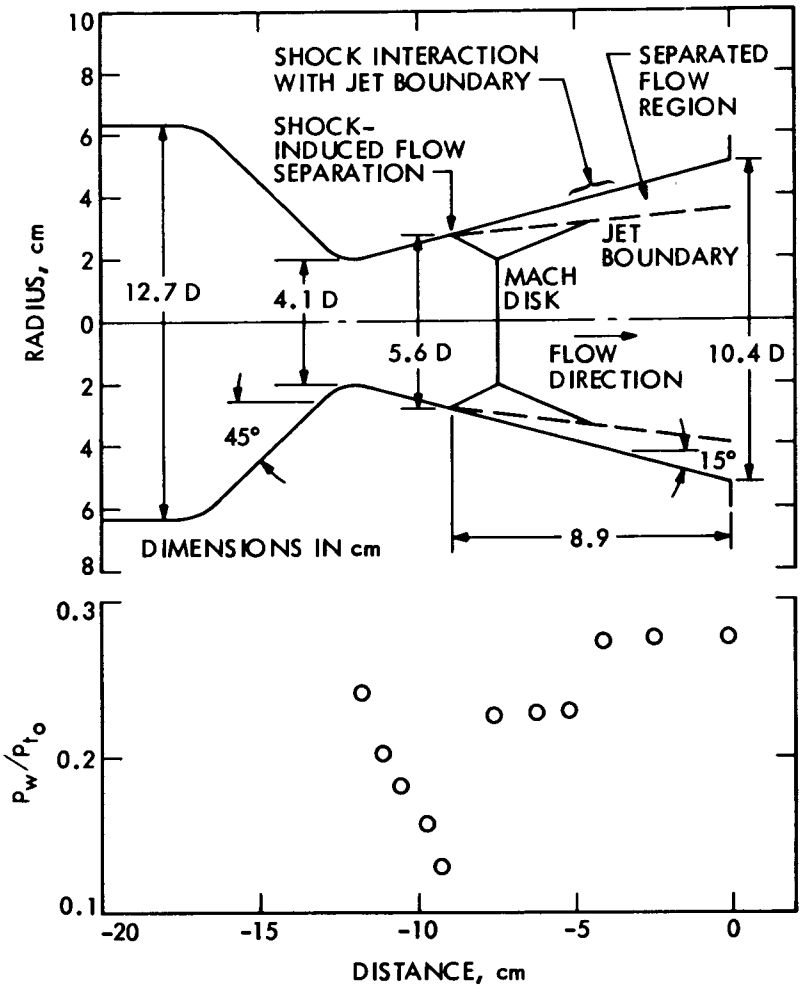

Figure 3. Nozzle Flow Field

the transonic flow field in terms of radial and axial distributions of Mach No. as determined experimentally is given in Ref. 6. The existance of additional weak oblique shock waves (not shown in Fig. 3) which emanated from a location near the tangency between the circular-arc throat and the conical divergent section is discussed in Ref. 7. Flow separation and reattachment that occurred in the vicinity of the curved inlet section when the nozzle inlet was attached to a constant-diameter duct upstream is presented in Ref. 8. Additional flow information together with wall heat transfer measurements which show the boundary layer laminarization effects appear in Ref. 9.

The jet was steady during the experiments discussed here and did not oscillate about the centerline of the nozzle. Such oscillations did occur at lower stagnation pressures when the flow separation point was farther upstream; however, no data was acquired under those conditions.

The origin of the "free jet", although contained, was actually inside the nozzle downstream of the flow separation point. In the laser beam and in the noise analyses the distances along the flow (x-direction), however, are referenced to the nozzle exit plane. Just downstream of the Mach disk the diameter of the jet was estimated to be about 6 cm and the Mach No. was 0.5. The jet velocity corresponding to this Mach No. is 310 m/sec. The velocity at the nozzle exit plane was probably somewhat lower; however, its value was not determined. For convenience the flow conditions are given in Table 1. All of the shock waves were contained within the nozzle. No such waves were observed in the jet downstream of the exit plane with Schlieren and shadowgraph systems that were used for this purpose.

Table 1

Flow Conditions, and Laser Beam and Microphone Locations

Jet Diameter D, at Flow Separation (Fig. 3) = 5.6 cm

Mach No. at Flow Separation (Fig. 3) = 2.2

Mach No. Downstream of Normal Shock (Fig. 3) = 0.5

Velocity Downstream of Normal Shock (Fig. 3) = 310 m/sec

Average Nozzle inlet stagnation pressure = 3.48 bar (50.4 psia)

Average Nozzle inlet stagnation temperature = 1100°K (1520°R)

Anechoic chamber pressure = 0.98 bar (14.2 psia)

Location of Vertical Laser Beam				Locations of Horizontal Laser Beams			
						Five beams for each value of ξ	
Test No.	x cm	x*/D	y cm	x cm	ξ cm	z cm	Radius cm
87	28.8	6.7	2.0	28.8	0	6.5	6.8
88	↓	↓	↓	29.8	1.0	2.5	3.2
89				31.8	3.0	-1.8	2.7
90				34.8	6.0	-5.4	5.8
						-9.8	10.0
96	66.4	13.4	2.1	67.2	0.8		
97	↓	↓	↓	68.2	1.8	6.7	7.0
98				69.2	2.8	2.7	3.4
99				66.4	0	-1.6	2.6
100				71.4	5.0	-5.2	5.6
101				73.4	7.0	-9.6	9.8
102				76.2	9.8		

Location of Vertical Laser Beam				Locations of Horizontal Laser Beams			
						Five beams for each value of ξ	
Test No.	x cm	x*/D	y cm	x cm	ξ cm	z cm	Radius cm
103	121.8	23.3	3.0	121.8	0		
104	↓	↓	↓	122.8	1.0	6.6	6.6
105				123.8	2.0	2.6	2.6
106				124.8	3.0	-1.7	1.7
107				125.8	4.0	-5.3	5.3
108				127.8	6.0	-9.7	9.7
109				129.8	8.0		

Locations of Microphones (Nos. 1 through 8 on 60 cm dia. circle)

Test No.	Microphone No. (Fig. 2)	β Deg.	Distance From Nozzle Exit to Microphone, cm
49	9	78	165
41	10	62	175
28	11	45	142
23	12	35	224
20	13	25	271
19	14	19	270

6. JET FLOW FIELD

The radial distribution of the mean value of the jet velocity U, was determined from measurements of the stagnation pressure, the static pressure and the stagnation temperature. This velocity distribution, vertically across the diameter, is shown in Fig. 4 at a distance of 116 cm downstream of the nozzle exit plane. This distance is about 22 jet diameters downstream of the flow separation location in the nozzle with the jet diameter based on the flow separation diameter shown in Fig. 3. It is evident that at this axial location the maximum jet velocity was about 110 m/sec (M_j = 0.27) and that the diameter of the jet had grown to about 60 cm. The region of highest shear (maximum $\partial U/\partial y$) at this axial location occurred over a radial distance between about 5 and 15 cm. The ratio of the jet mass flux to nozzle mass flux was 13.6.

Also shown in Fig. 4 is the radial distribution of the convection velocity of the eddies U_c, which was determined from laser beam measurements at five positions spaced vertically across the diameter of the jet. The data shows that both the jet velocity and the eddy velocity are reasonably symmetrical about the centerline of the jet. Additional results of the convection velocity are discussed in the next section.

Radial distributions of the stagnation pressure, stagnation temperature and static pressure referenced to ambient conditions are shown in Fig. 5. It should be noted that the static pressure in the flow is below ambient pressure, even this far downstream. If it had been assumed that the static pressure were the same as the ambient pressure, the maximum velocity would have been calculated to be about 7 per cent lower than shown in Fig. 4 and the diameter of the jet would have been about 13 per cent smaller.

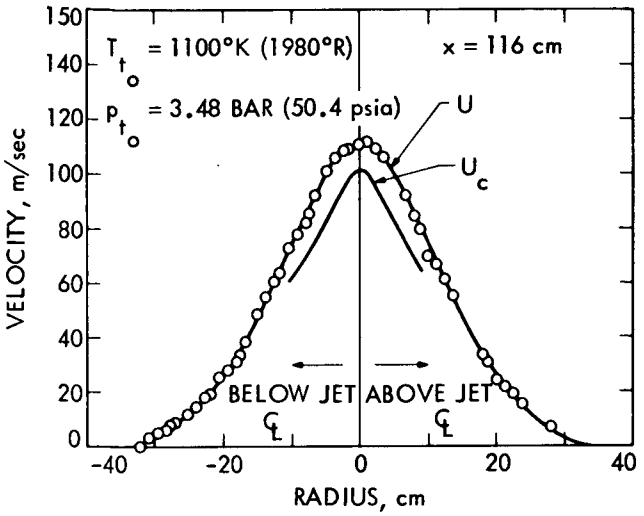

Figure 4. Radial Distributions of Mean Velocity and Convection Velocity

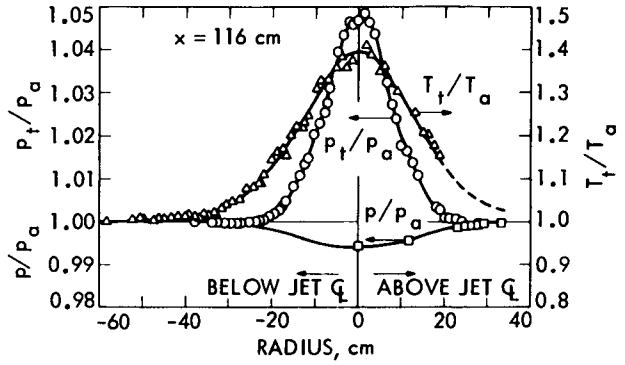

Figure 5. Radial Distributions of Pressure and Temperature

7. CONVECTION VELOCITY

The convection velocity of the eddies U_c, was evaluated at the axial locations where laser beam measurements were made (Fig. 2). It was determined by the separation distance of the laser beams ξ, divided by the appropriate time delay τ, and is based on the loci of the tangent points of the envelope curve for the experimental cross correlations. A comparison of the radial distribution of the convection velocity with the jet velocity is shown in Fig. 4 at a distance of 116 cm from the nozzle exit plane. It is evident that the distributions follow the same trends. At the centerline the ratio of the convection velocity to the jet velocity is 0.9 and near the outer limits of the convection velocity curve shown, the ratio of local convection velocity to local jet velocity is more nearly 0.8. Radial distributions of the convection velocity at the other axial locations are shown in Fig. 6. The distributions are essentially symmetrical about the centerline and the peak values decrease along the flow direction. The crossover of the curves near the outer edges is a result of the spreading of the jet as the distance from the nozzle exit plane increases.

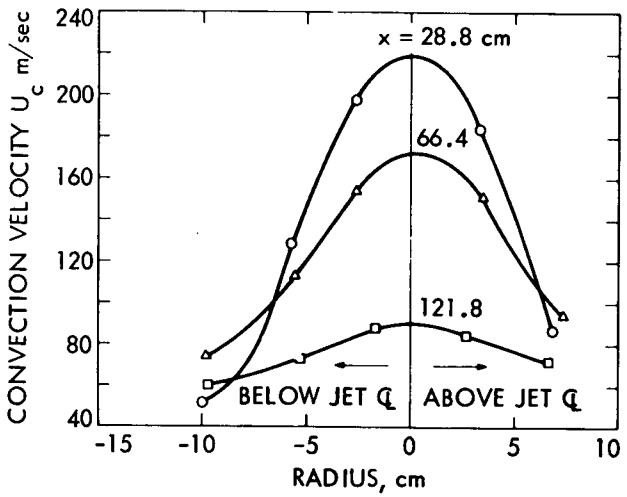

Figure 6. Radial Distributions of Convection Velocity

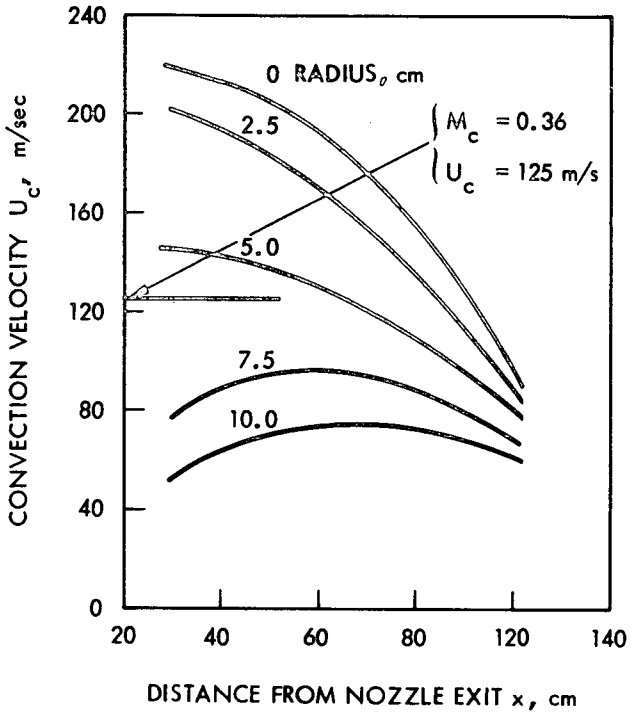

Figure 7. Axial Distributions of Convection Velocity

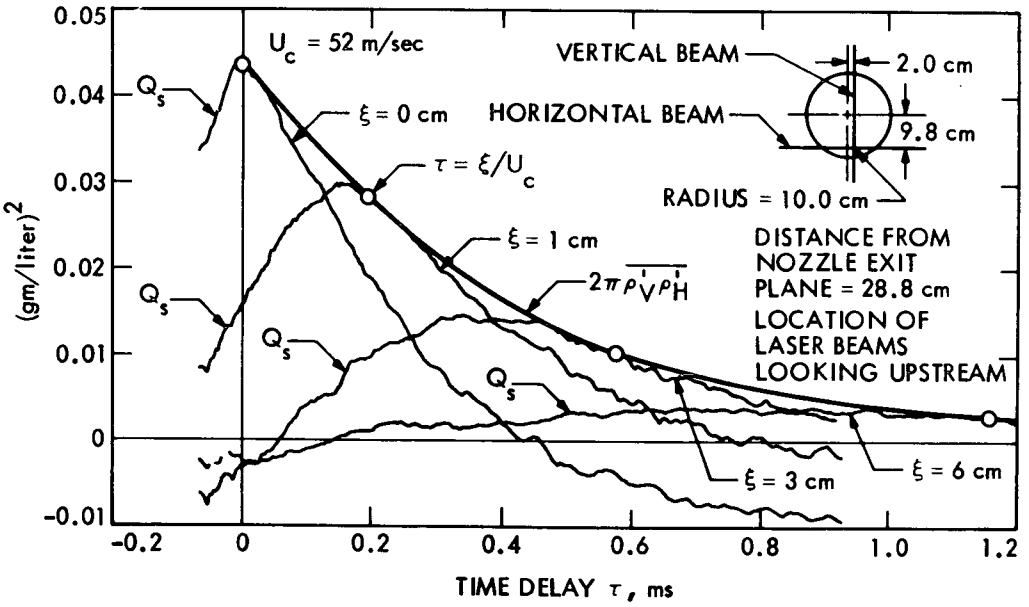

Figure 8. Experimental Correlations of Fluctuating Density vs Time Delay

Distributions along the axial direction at various radii are shown in Fig. 7. At the larger radii the convection velocity would be zero at the nozzle exit (outside the jet). Farther downstream as the jet spread to the particular radius, at which a measurement is being made, the velocity of the eddies would be observed. A maximum value would be expected before the velocity decayed. Such a trend is apparent at radii of 7.5 and 10 cm. Near the centerline there was a continuous decay. A convection velocity of 125 m/sec, which is based on an average throughout the jet, was chosen for evaluation of the noise autocorrelation function in the moving reference frame.

8. EXPERIMENTAL DENSITY FLUCTUATIONS

Typical cross correlations Q_s, of the density fluctuations vs time delay τ, are shown in Fig. 8. At zero separation distance of the vertical and of the horizontal beams ($\xi = 0$) the curve is symmetric about $\tau = 0$. A decay in the intensity, that is, in the peak values of the curves, occurs as the separation distance is increased. The upper envelope of this family of curves is a smooth function as shown. It is the autocorrelation function $2\Pi \overline{\rho_V' \rho_H'}$ in the moving frame of reference of the eddies, that is, $2\Pi Q$, or also; it is the Fourier transform of the fluctuating density spectrum. The locations of the laser beams are shown in the sketch in the upper right-hand corner of Fig. 8. The radius of the measuring station was 10.0 cm. At this axial location of x = 28.8 cm the results obtained at other horizontal beam positions resemble those shown in Fig. 8. The peak correlation values differ, however, as does the steepness of the cross correlation curves, and, of course, the convection velocity.

Distributions across the jet of the rms density fluctuations are shown in Fig. 9 at three axial locations. The position of the vertical beam was about 2 cm off-axis for the two upstream locations as shown in Fig. 2 and given in Table 1, but it was on the axis for the farthest downstream location. At the farthest upstream location (x = 28.8 cm), where the stagnation temperature on the axis of the jet was estimated to be about 1000°K, the ratio of the rms density fluctuation, at a radius of 10 cm, to the mean density at the centerline was 0.21. At the farthest downstream location (x = 121.8 cm), where the stagnation temperature on the jet axis had decreased to about 400°K, the ratio of the rms fluctuating density to the mean density on the jet axis had decayed to 0.008. Minima which occur in the horizontal plane passing through the center of the jet are inferred from the curves. At 28.8 cm the distance from the flow separation location is about 7 jet diameters based on the flow separation diameter. At 66.4 cm this distance is about 13 jet diameters. The larger fluctuations at 13 jet diameters do not contribute as much to the radiated noise as do the fluctuations farther upstream. This is deduced from the results of the noise data discussed in the next section. There, it is evident that the maximum noise intensity occurred at about 4 jet diameters from the flow separation location and that farther downstream there was a continuous decrease in noise intensity. Thus, further clarification is needed before a relationship between the density fluctuation and the radiated noise can be established.

The largest density fluctuations occurred at the larger radial measuring stations of the jet, as shown in Fig. 9, in the region of the highest shear. At the farthest location downstream, about 23 jet diameters, the distribution is essentially uniform even in the region of maximum shear. This farthest downstream position is very near the location at which the radial distribution of the velocity is shown in Fig. 4.

Distributions of the most significant variables related to the fluctuating density are shown in terms of the peak rms fluctuating density (Fig. 9), the convection velocity (Fig. 4), and the time scale of the moving density autocorrelation, which is the time delay at which the rms density fluctuation has a value equal to one-half of its maximum value (Fig. 10). This time scale is nearly constant in the central region across the jet but is larger at the radius of 10 cm, which corresponds to the radius of the Fig. 8 results. In the central region of the jet the time scales are typically about 0.25 milliseconds; whereas,

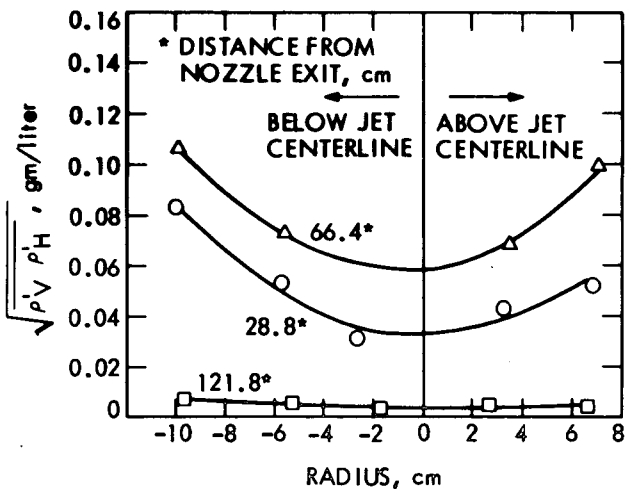

Figure 9. Distributions of rms Density Fluctuations at $\xi = 0$

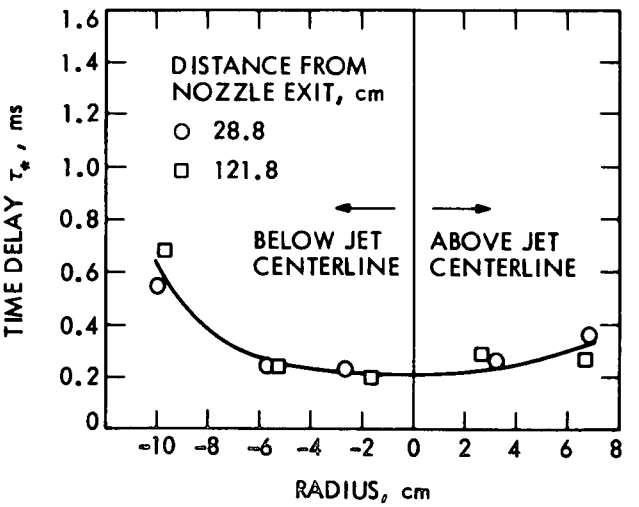

Figure 10. Time Scale Distribution

the corresponding time delay scale of the moving noise source is more nearly 0.1 millisecond as deduced from the noise correlations discussed in the next section. The density fluctuation correlations, however, should not be compared directly with the noise correlations. Instead, as discussed in Appendix A2, it is the second derivative of the $\overline{\rho_V' \rho_H'}$ fluctuations with respect to time delay τ, which is related to the density autocorrelation Ψ_d, and hence to the noise autocorrelation Ψ_n. Additional experimental data is required before this can be done with sufficient accuracy.

The decay of the rms value of the density fluctuations vs beam separation along the flow is shown in Fig. 11. These results are given at only three radii at each axial location for clarity but indicate typical trends. The higher rms values at x = 66.4 cm at the larger radii are evident in this figure also. It is apparent that the decay in intensity of the eddies in the high shear region (outer radii) occurs over a comparatively short distance.

In the experiments the two-point correlation of the density fluctuation Q, was evaluated from the crossed laser beam measurements at several locations. From these values of Q the second time derivative, which is related to the density autocorrelation, was obtained by means of a computer program. An example of the second time derivative is shown in Fig. 12. In this figure the most important result is the maximum value, which occurs at zero time delay. The location at which the curve crosses the horizontal axis is shown also. The significance of the peak value is that it can be introduced into Eq. (A2-22) together with the mean velocity gradient to obtain the fluctuating density autocorrelation function Ψ_d. Then the relationship between the fluctuating density inside the jet and the noise radiated outside can be established by the relationship between Ψ_d and Ψ_n. The evaluation of Ψ_n is discussed in the next section. Determination of the relationship between Ψ_d and Ψ_n, however, is beyond the scope of this investigation.

9. RADIATED NOISE

The noise radiated from the jet is presented in two ways, first in terms of a 1/3 octave band analysis compared with Lighthill's theory of convected quadrupoles (Ref. 1) together with a comparison of some of the cold flow data of Lush (Ref. 2), and second it is characterized in terms of the noise cross correlation coefficient as well as the autocorrelation function in the moving reference frame of the eddies.

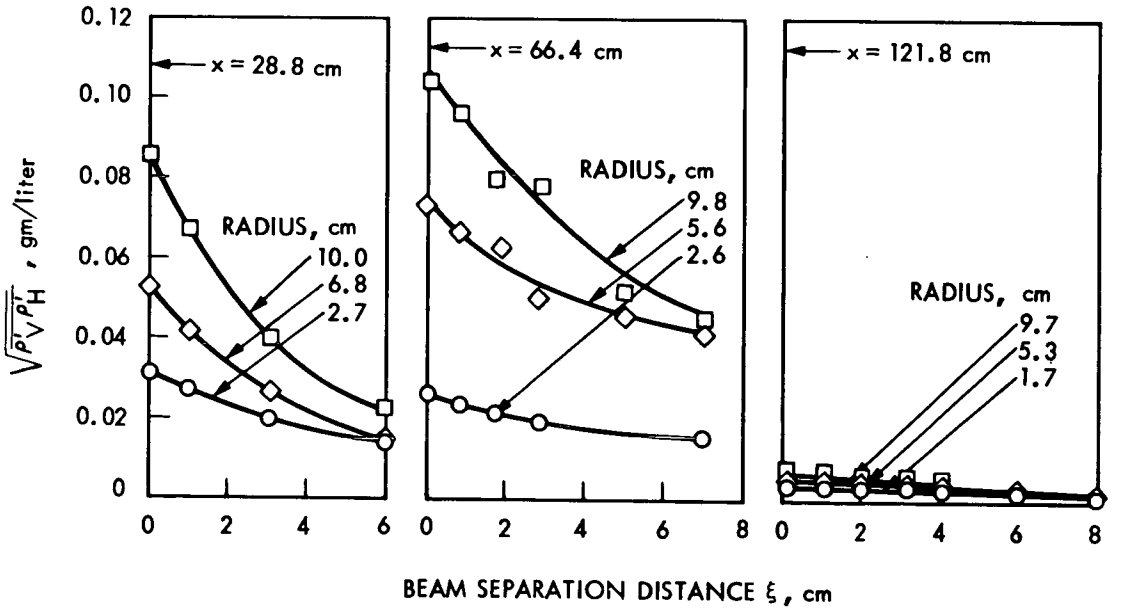

Figure 11. Decay of Density Fluctuations vs Beam Separation

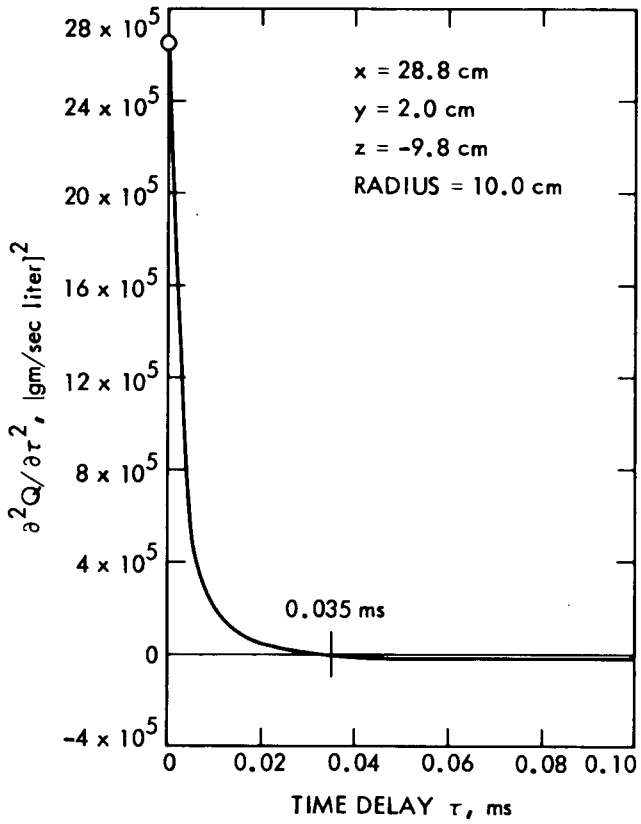

Figure 12. Second Time Derivative of the Density Fluctuation Correlation

In Fig. 13 the differences in sound pressure levels between Lighthill's theory and the experimental values are shown as a function of the non-dimensional frequency parameter fD/a_o, for various values of the emission angle θ. The experiments were conducted for only one value of nozzle exit velocity; hence,

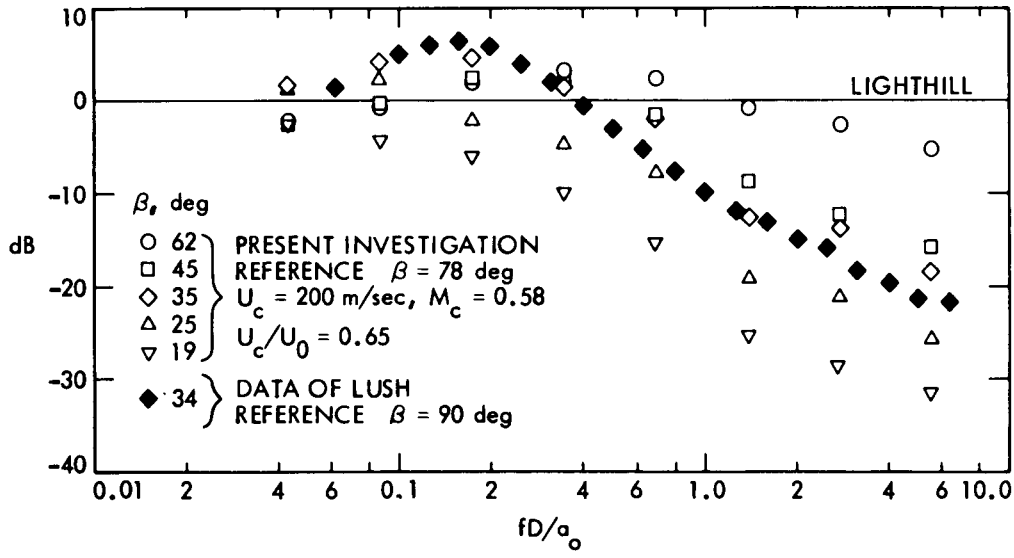

Figure 13. Comparison of Differences in Sound Pressure Levels With Lighthill's Theory

comparisons over a velocity range are not made. The experimental results shown were obtained with microphone Nos. 9 through 14 shown in Fig. 2. The locations of these microphones are given in Table 1. In order to be consistent with the model of convected sources the observed frequency is corrected for a Doppler shift so that the same source frequency is examined for any emission angle. The equation for this relationship in terms of the intensity referenced to an emission angle of 90° is

$$I(f,\beta) = \frac{R_{90}^2}{R_\beta^2} \frac{I\left(f\left\{[1 - M_c \cos\beta]^2 + \alpha^2 M_c^2\right\}^{\frac{1}{2}}, 90^\circ\right)}{\left\{[1 - M_c \cos\beta]^2 + \alpha^2 M_c^2\right\}^{5/2}} \tag{2}$$

Equation (2) is based on Lighthill's prediction for the far field intensity of the noise generated by a turbulent flow as modified by Ffowcs Williams (Ref. 10) to apply to the noise radiated from a jet. See also the discussion by Lush (Ref. 2).

Lush showed good agreement between Lighthill's theory and his experimental results for emission angles near 90° over a significant range of the frequency parameter. The data of the present investigation is referenced to an emission angle of 78° which is considered sufficiently near 90° for extrapolation to 90° without much loss in accuracy. Thus for the reference condition of $\beta = 78^\circ$ Eq. (2) becomes

$$I(f,\beta) = \frac{R_{78}^2}{R_\beta^2} \frac{I\left(f\left\{\frac{[1 - M_c \cos\beta]^2 + \alpha^2 M_c^2}{[1 - M_c \cos 78]^2 + \alpha^2 M_c^2}\right\}^{\frac{1}{2}}, 78\right)}{\left\{\frac{[1 - M_c \cos\beta]^2 + \alpha^2 M_c^2}{[1 - M_c \cos 78]^2 + \alpha^2 M_c^2}\right\}^{5/2}} \tag{3}$$

The data of the present experiments shown in Fig. 13 were corrected with the use of Eq. (3). Furthermore, the convection velocity U_c, was chosen to be 200 m/sec. Thus $M_c = 0.58$. This selected value of U_c is based on the distributions shown in Fig. 7. At the nozzle exit ($x = 0$) the radius of the jet was about 3 cm; hence $U_c \simeq 200$ m/sec and since $U_0 \simeq 310$ m/sec, $U_c/U_0 = 0.65$. This is the same value of U_c/U_0 used by Lush who made use of the results obtained by Davis, Fisher and Barratt (Ref. 11). The quantity α was chosen to be 0.3 as used by Lush.

The results in Fig. 13 indicate that for low angles and high frequencies Lighthill's prediction (the zero dB line) is higher than the experimental data. This probably occurs because of the absence of appropriate accountability in the theory for the effects of refraction of the noise by the flow, and of the convection amplification which results from the source moving with the flow or more slowly than the flow. At low frequencies the experimental results are in reasonably good agreement with the theory especially at the larger angles; however, there is still an effect of the emission angle at the smaller angles. The comparison of the results at $\beta = 35^\circ$ with that of Lush at $\beta = 34^\circ$ is quite good over the entire frequency parameter range despite the significant difference in the stagnation temperatures of the two sets of data. This is the only emission angle common to the data of Lush and to the data of the present investigation.

Characterization of the radiated noise in terms of the autocorrelation function $n\psi_n$, in the moving frame of reference of the eddies is shown as a three-dimensional display in Fig. 14. In this case the convection velocity was chosen to be 125 m/sec ($M_c = 0.36$), instead of 200 m/sec, because the lower value is more nearly a mean value over the extent of the jet as can be seen in Fig. 7. The effect of the convection velocity on the results is largely associated with the relationship between the time t, and the distance x. Since the correlation is determined primarily from geometric considerations, the distance scale in Fig. 14 would not be affected very much by such a difference in velocity but the time scale would. The autocorrelation function $n\psi_n(t, \Delta t)$ reaches a maximum at about 13 cm downstream of the nozzle exit plane and then decays to a small value in about 5 milliseconds or approximately 63 cm from the nozzle. These distances correspond to about 4 and 13 jet diameters respectively from the flow separation location inside the nozzle. The method of evaluating this autocorrelation function is discussed in Appendix A3 and is demonstrated by the use of numerical values in the next paragraph. To acquire the cross correlations from which these results were obtained eight microphones were located in a circle as shown in Fig. 2. The angular region β, covered by the circular array, was between about 35 and 55°. The effects of refraction and convection amplification are, of course, included in the experimental results even though the moving point-source theory does not take these effects into account.

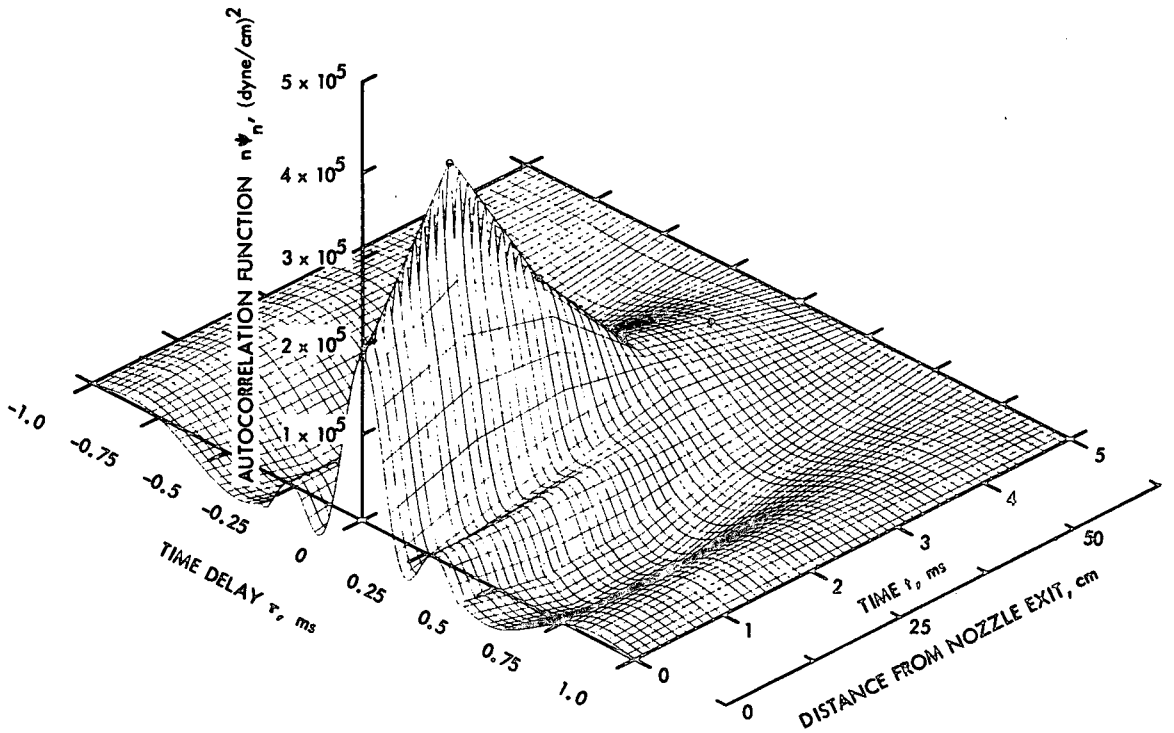

Figure 14. Autocorrelation Function of the Radiated Noise

The following numerical example is a description of the method that was used to compute the autocorrelation function shown in Fig. 14. A constant convection velocity of the eddies was assumed although allowance for a variable velocity could be incorporated into the procedure. Three frequency bands centered at 1, 3, and 9 kHz with $\alpha = 3$ were used to evaluate $\phi_1(\Delta t)$ using Eq. (A3-3) in Appendix A3. Note that this α refers to frequency bands of Eq. (A3-3) and differs from the α of Eqs. (2) and (3). For $\alpha = 3$, the bandwidth is about 1.6 octaves. The time increment δ, which was used to evaluate $g_1(t_2)$ in Eq. (A3-2) was 1.0 ms. Five increments were used which made it necessary to determine g_1 at 6 nodal points.

The experimental correlations $C(\tau)$, were evaluated from the signals of the following pairs of microphones shown in Fig. 2: 1 and 5, 2 and 6, 3 and 7, and 8 and 4. Also, the autocorrelation of microphone No. 1 (1 and 1 with time delay) was used. As an example of the shapes of these curves the experimental cross correlation for Nos. 8 and 4 and the autocorrelation of No. 1 and 1 with time delay are shown in Figs. 15 and 16. A fixed value of τ and a particular orientation of a microphone pair determine a line in the $\Delta t, t_2$ plane. The correlation $C(\tau)$ is a line integral of $n\Psi_n$ along this line. To obtain information about $n\Psi_n$ in various regions in this plane, different varieties of such paths (and therefore different orientations of microphones) were chosen. Points were then taken from each of these correlation curves at different values of time delay τ, thereby establishing a set of simultaneous equations. In theory, only a total of 18 values was required to evaluate the unknown coefficients since the number of nodal points chosen was 6 and the number of frequency bands was 3. However, a total of about 100 was used for better smoothing since the computation method involved the use of inversion by least squares. The source function in terms of the frequency and time, i.e., $n\Psi_n(f_1, t_2)$, obtained by this method for the three bands (Ref. 12) is consistent with observed trends for subsonic jets. For example, the noise sources at higher frequencies occur near the nozzle exit and the lower frequencies extend over a larger distance along the jet.

A check on the inversion by least squares of the computation method using the coarse time step was obtained by inserting the computed coefficients into Eq. (A3-1) and calculating values of $C(\tau)$. These computed values are shown in Figs. 15 and 16 for comparison with the experimental values. It is evident that the agreement is very good and hence, that the inversion gives good results.

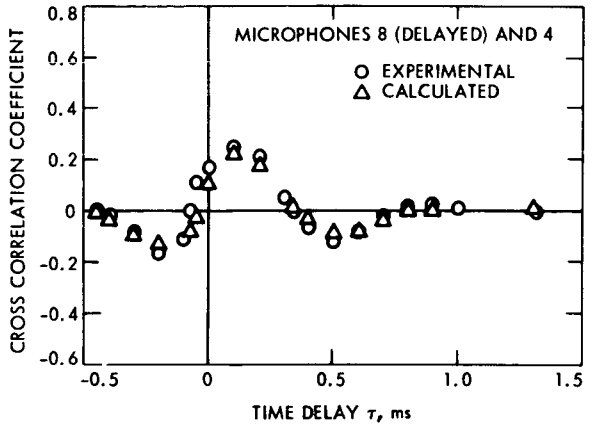

Figure 15. Comparison of Calculated Cross Correlation Coefficients with Experimental Values

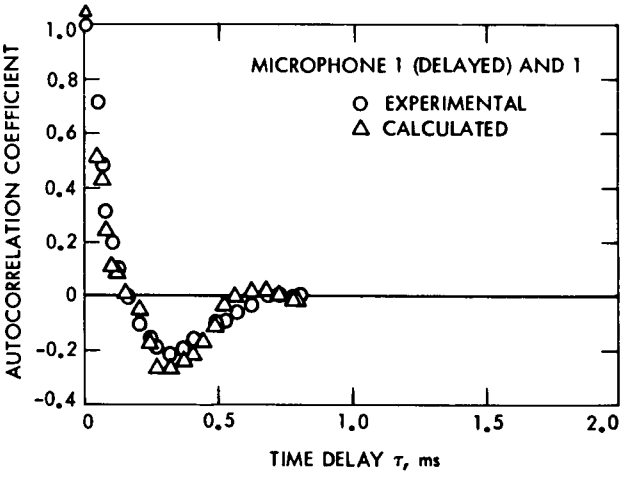

Figure 16. Comparison of Calculated Autocorrelation Coefficient with Experimental Values

10. CONCLUDING REMARKS

In this investigation experiments were conducted on a high-temperature subsonic jet which separated at a supersonic velocity inside the divergent portion of a nozzle. The separated jet flow progressed through a shock structure contained entirely within the nozzle and then became subsonic before it reached the nozzle exit plane.

It was demonstrated from measurements obtained within the jet flow outside the nozzle using spatially separated crossed laser beams set up as a Schlieren system that the noise sources can be characterized by radial and axial distributions of the convection velocity, the magnitude of rms density fluctuations, and by correlations of the density fluctuations in the moving frame of reference of the eddies. Likewise, the radiated noise was characterized by correlations of signals detected from pairs of spatially separated microphones outside the jet. Based on this measurement technique of the radiated noise combined with the use of the convection velocity, the autocorrelation function of the noise in the moving reference frame of the eddies was evaluated together with the noise intensity and its spectral distribution. The analyses of the noise sources and of the radiated noise are based on moving point sources in the jet. A feature of these approaches is that they will lead to the determination of a relationship between the noise sources inside the jet and the radiated noise outside the jet based on experimental measurements.

Comparisons of the experimental noise results with Lighthill's theory of convected quadrupoles indicates good agreement at the lower frequencies, especially at the larger emission angles. At low angles and at high frequencies Lighthill's prediction is higher than the data. It is believed that this difference results primarily from neglecting the effects of refraction and of limitations in the accountability of convection amplification in the theory. The experimental noise results at one common emission angle agree quite well with the data of Lush even though there was a large difference in the stagnation temperatures of the jets investigated.

11. REFERENCES

1. M. J. Lighthill, "On Sound Generated Aerodynamically," Part I, "General Theory," Proceedings of the Royal Society (London), Series A, Vol. 211, No. 1107, March 20, 1952, pp. 564-587.

2. P. A. Lush, "Measurements of Subsonic Jet Noise and Comparison With Theory," Journal of Fluid Mechanics, Vol. 46, Part 3, April 13, 1971, pp. 477-500.

3. M. J. Lighthill, "On Sound Generated Aerodynamically," Part II, "Turbulence as a Source of Sound," Proceedings of the Royal Society (London), Series A, Vol. 222, No. 1148, February 23, 1954, pp. 1-32.

4. P. F. Massier and S. P. Parthasarathy, "An Anechoic Chamber Facility for Investigating Aerodynamic Noise," Technical Report 32-1564, Jet Propulsion Laboratory, Pasadena, California, September 15, 1972.

5. L. H. Back, P. F. Massier and R. F. Cuffel, "Heat Transfer Measurements in the Shock-Induced Flow Separation Region in a Supersonic Nozzle," AIAA Journal, Vol. 6, No. 5, May 1968, pp. 923-925.

6. R. F. Cuffel, L. H. Back and P. F. Massier, "Transonic Flow Field in a Supersonic Nozzle with Small Throat Radius of Curvature," AIAA Journal, Vol. 7, No. 7, July 1969, pp. 1364-1366.

7. L. H. Back and R. F. Cuffel, "Detection of Oblique Shocks in a Conical Nozzle with Circular-Arc Throats," AIAA Journal, Vol. 4, No. 12, December 1966, pp. 2219-2221.

8. L. H. Back, P. F. Massier and R. F. Cuffel, "Flow and Heat Transfer Measurements in Subsonic Air Flow Through a Contraction Section," International Journal of Heat and Mass Transfer, Vol. 12, No. 1, January 1969, pp. 1-13.

9. L. H. Back, P. F. Massier and R. F. Cuffel, "Flow Phenomena and Convective Heat Transfer in a Conical Supersonic Nozzle," Journal of Spacecraft and Rockets, Vol. 4, No. 8, August 1967, pp. 1040-1047.

10. J. E. Ffowcs Williams, "The Noise From Turbulence Convected at High Speed," Royal Society of London, Philosophical Transactions of the Royal Society (London), Series A, Vol. 255, 1962-1963, pp. 469-503.

11. P. O. A. L. Davies, M. J. Fisher and M. J. Barratt, "The Characteristics of the Turbulence in the Mixing Region of a Round Jet," Journal of Fluid Mechanics, Vol. 15, March 1963, pp. 337-367.

12. S. P. Parthasarathy, "Evaluation of the Noise Autocorrelation Function of Stationary and Moving Noise Sources by a Cross Correlation Method," AIAA Paper No. 73-186, January 10-12, 1973.

13. L. N. Wilson and R. J. Damkevala, "Statistical Properties of Turbulent Density Fluctuations," Journal of Fluid Mechanics, Vol. 43, August 1970, pp. 291-303.

12. ACKNOWLEDGEMENTS

The authors greatly appreciate the assistance of Mr. F. H. Slover and Mr. S. J. Kikkert in conducting the experiments, in assembling the test apparatus and in analyzing the data.

Appendix

A 1 AUTOCORRELATION FUNCTIONS OF A MOVING NOISE SOURCE

Autocorrelation functions for the fluctuating density of a moving noise source can be determined for a jet flow from measurements obtained by the crossed-beam laser-Schlieren method described in Appendix A2. In addition, such functions for the radiated noise can be determined from the cross correlations of the signals detected by a pair of microphones as described in Appendix A3. The moving source autocorrelation functions are important because they can be used to obtain a description of the entire noise field. In the moving reference frame fluctuations occur more slowly; hence, greater accuracy in time derivatives is obtainable. Thus the intensity and spectrum of the fluctuating density within the jet and the intensity and spectrum of the noise, which is related to the radiated sound pressure outside the jet, can be evaluated.

The autocorrelation function in the moving frame of reference of the eddies may be determined as follows: First, let $G(\underline{x},t)$ be a fluctuating random scalar function in the turbulent jet flow. In the present investigation, for example, it would represent the fluctuating density. At every point $\underline{x}$ a convection velocity $\underline{U}_c(\underline{x})$ is defined. If now a hypothetical probe is considered which senses a fluctuating quantity and which follows the motion of the eddies at the convection velocity, the signal observed would be given by $G(\underline{x}_0 + \int_0^t \underline{U}_c\, dt, t)$ where $\underline{x}_0$ is the initial position. Thus the quantity G, is a function of time only because $\underline{x}$ is a function of time taken along the trajectory of the probe.

The autocorrelation function obtained from the signals at different times (different locations) for a probe moving at the velocity $\underline{U}_c$, is given by the ensemble average of G as follows:

$$< \left[G\left(\underline{x}_0 + \int_0^t \underline{U}_c\, dt, t\right)\right] \left[G\left(\underline{x}_0 + \int_0^{t+\tau} \underline{U}_c\, dt, t+\tau\right)\right] >$$

The measurement obtained from the probe at one time after having been delayed by a time interval τ is multiplied by the measurement from the same probe obtained sometime later. If it is assumed that $G(\underline{x},t)$ is locally homogeneous and locally stationary, that is the mean value of G is not changing with time,

$$< G\left(\underline{x}_1, t_1\right) G\left(\underline{x}_2, t_2\right) > = \Psi\left(\underline{x}_1, t_1; \underline{x}_2 - \underline{x}_1, t_2 - t_1\right) \qquad \text{(A1-1)}$$

Ψ is a slowly varying function of $\underline{x}$ and t when the flow is approximately homogeneous and approximately stationary. For jets that are strictly stationary there is only a slow change of Ψ with $\underline{x}$ and for this case the right side of Eq. (A1-1) is equal to

$$\Psi\left(\underline{x}_1; \underline{x}_2 - \underline{x}_1, t_2 - t_1\right) \text{ or } \Psi\left(\underline{x}; \int_0^{t+\tau} \underline{U}_c dt, \tau\right),$$

that is,

$$\Psi\left(\underline{x}_o + \int_0^t \underline{U}_c\,(t)dt; \underline{U}_c\,(t)\tau, \tau\right).$$

This varies slowly with t and rapidly with τ. The coordinate $\underline{x}_0$ refers to the initial point at the nozzle exit. This is the function which is obtained from the laser beam cross correlations described in Appendix A2. There, the method of obtaining the autocorrelation function in the moving frame of reference is developed from the measurements of signals detected by the use of stationary beams. The noise autocorrelation function is converted to the moving reference frame by introducing the value of U_c determined from the laser data.

A 2 LASER SCHLIEREN ANALYSIS

This discussion pertains to the evaluation of the autocorrelation function of the fluctuating density for an observer that moves along the jet flow at the convection velocity of the eddies. The autocorrelation function in this moving frame of reference can be obtained from the detected signals emitted by stationary laser beams. This can be done either if several beams are displaced along the flow direction or else if one of the beams is moved to different positions at which data is obtained. The analytical procedure that will be followed is an extension of that used by Wilson and Damkevala (Ref. 13). A sketch of a typical arrangement is shown in Fig. A 2-1.

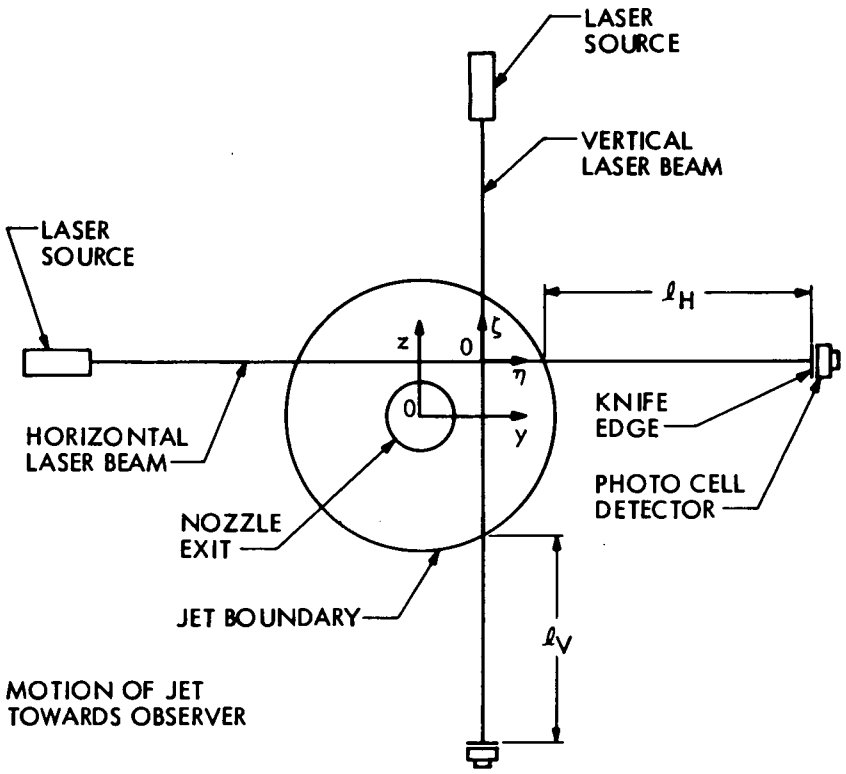

Figure A 2-1. Laser-Schlieren Arrangement

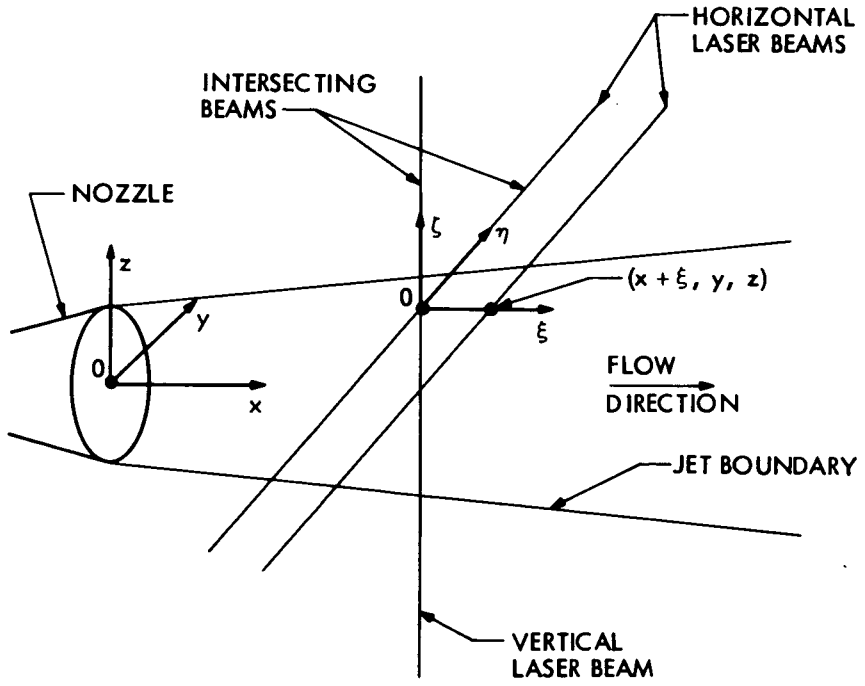

Figure A 2-2. Coordinate Axes x, y, z and ξ, η, ζ

As shown in Fig. A 2-1 the origin of the coordinates x, y and z is on the centerline of the nozzle at the nozzle exit plane. This figure represents a view looking upstream into the jet. Also, the coordinates ξ, η and ζ are in the directions x, y and z respectively but their origin is at the location where the vertical and the horizontal laser beams intersect. If the vertical and the horizontal beams are separated, this origin is located on the vertical beam at the intersection with a horizontal plane passed through the horizontal beam. Thus, the displacement of a horizontal beam along the flow direction from the vertical beam is taken to be $+\xi$. The coordinates in three dimensions are shown in Fig. A 2-2.

As the beam passes through the jet it is deflected wherever there is a gradient in the refractive index. It can be shown that if n is the refractive index, the angular deflection γ, of the beam is given by

$$\gamma_H(t) = \int_{L_\eta} \frac{\partial n}{\partial x}\, d\eta \qquad \text{(A2-1)}$$

$$\gamma_V(t) = \int_{L_\zeta} \frac{\partial n}{\partial x}\, d\zeta \qquad \text{(A2-2)}$$

The subscripts H and V refer to the horizontal and to the vertical beams respectively. The dimensions L_η and L_ζ represent those portions of the beam lengths which lie within the jet diameter. Gradients of the refractive index in Eqs. (A2-1) and (A2-2) are taken along the flow direction because it is only the deflections that result from these gradients that will give correlations. If gradients perpendicular to the flow are sensed, Schlieren signals will be obtained; however, their cross correlations would be zero. Thus the knife edges of the Schlieren system must be aligned perpendicular to the flow for both the vertical and the horizontal beams.

The output signals of the Schlieren detectors may be expressed as follows:

$$e_H = S_H \ell_H \gamma_H \qquad \text{(A2-3)}$$

$$e_V = S_V \ell_V \gamma_V \qquad \text{(A2-4)}$$

S is the sensitivity and ℓ the beam length between the edge of the jet and the detector (Fig. A 2-1). The signal from the horizontal beam is delayed by a time interval τ, and thereby a correlation with the other signal is obtained which is the average of the product of the angular deflections as follows:

$$\langle \gamma_H (t - \tau)\, \gamma_V (t) \rangle = \int_{L_\eta} \int_{L_\zeta} \left\langle \left[\frac{\partial n}{\partial x}(t - \tau)\right]_\eta \left[\frac{\partial n}{\partial x}(t)\right]_\zeta \right\rangle d\eta d\zeta \qquad \text{(A2-5)}$$

The relationship between the refractive index and the density is $\partial n/\partial x = \epsilon\, [\partial \rho/\partial x]$ where ϵ is the Gladstone-Dale constant. Then, if Q_s is defined as the experimentally determined cross correlation function, its value in terms of the density gradient is established by combining Eqs. (A2-3) and (A2-4) to eliminate γ and n, and by introducing the relation between the refractive index and the density. For convenience, the quantities obtained from measurements are grouped together and equated to those quantities under the integrals that are to be determined. Thus

$$\frac{\langle e_H(t - \tau)\, e_V(t) \rangle}{S_H S_V \ell_H \ell_V \epsilon^2} \equiv Q_s(x,y,z,\xi,\tau) = \int_{L_\eta} \int_{L_\zeta} \left\langle \frac{\partial \rho}{\partial x}(x, y + \eta, z, t - \tau)\, \frac{\partial \rho}{\partial x}(x + \xi, y, z + \zeta, t) \right\rangle d\eta d\zeta \qquad \text{(A2-6)}$$

In Eq. (A2-6) by denoting functions of $(y + \eta)$, $(x + \xi)$ and $(z + \zeta)$ it is assumed that in general the laser beams do not pass through the axis of the jet. However, this of course is not a requirement.

A2-1 Stationarity

Note that Q_s in Eq. (A2-6) is not a function of the time t, because of the stationarity of a real jet. This is a valid assumption because the time period t, is orders of magnitude larger than the time delay τ, which is measured in milliseconds.

A2-2 Homogeneity

If in addition to local stationarity the fluctuations are considered to be homogeneous over distances for which the correlation in the integrand contributes appreciably to the integral, that is, if there is a weak dependence on x, y and z but a strong dependence on ξ, η and ζ,

$$< \frac{\partial \rho}{\partial x}(x,y+\eta,z,t-\tau)\,\frac{\partial \rho}{\partial x}(x+\xi,y,z+\zeta,t) > = -\frac{\partial^2}{\partial \xi^2} < \rho(x,y,z,t)\,\rho(x+\xi,y-\eta,z+\zeta,t+\tau) >$$

$$\equiv -\frac{\partial^2}{\partial \xi^2} Q(x,y,z;\,\xi,\,-\eta,\,\zeta,\,\tau) \qquad \text{(A2-7)}$$

The defined quantity Q, is the two-point correlation function of the fluctuating density. In a real jet the condition of homogeneity is not strictly satisfied because of the growth in diameter along the flow direction (development of the flow with respect to position). Nevertheless, at beam locations downstream of the nozzle exit plane the influence of changes in ξ, η and ζ on the value of Q is much greater than is the influence of the same changes in x, y and z.

It is permissible to extend the limits of integration to the range of $-\infty$ to $+\infty$ because the correlation in the integrand vanishes for large distances of η and ζ, that is, beyond the boundaries of the eddy, which can be no larger than the jet. Thus, combination of Eqs. (A2-6) and (A2-7) gives

$$Q_s(x,y,z,\xi,\tau) = -\int_{-\infty}^{\infty}\int_{-\infty}^{\infty} \frac{\partial^2}{\partial \xi^2} Q(x,y,z;\,\xi,\,-\eta,\,\zeta,\,\tau)\,d\eta d\zeta \qquad \text{(A2-8)}$$

A2-3 Isotropy

The quantity to be determined in Eq. (A2-8) is the autocorrelation function Q; consequently, this equation must be inverted. In order to simplify this procedure the fluctuations will be considered to be isotropic. The assumption of isotropic fluctuations implies that fixed values of the cross correlation coefficient are spherical surfaces. Furthermore, it implies that as the eddies move downstream they become larger. Actually, however, the peak cross correlations become smaller; hence, the "sizes" (radii) of the spherical surfaces become smaller until they finally diminish. Nevertheless, by assuming isotropy Eq. (A2-8) becomes

$$Q_s(x,y,z;\,\xi,\tau) = -\int_{-\infty}^{\infty}\int_{-\infty}^{\infty} \frac{\partial^2}{\partial \xi^2} Q\left(x,y,z;\sqrt{[\xi - U_c\tau]^2 + \eta^2,\ \zeta^2},\ \tau\right) d\eta d\zeta \qquad \text{(A2-9)}$$

Note that in Eq. (A2-9) the quantity $[\xi - U_c\tau]^2$ has been substituted for ξ^2. U_c is the convection velocity of the eddies along ξ (the flow direction); therefore, by this substitution Eq. (A2-9) has been converted into the moving frame of reference of the eddies. The inversion can be accomplished by a change of variables and mathematical manipulation. Thus, define R and μ as follows:

$$R \equiv \sqrt{[\xi - U_c\tau]^2 + \eta^2 + \zeta^2} \qquad \text{(A2-10)}$$

$$\mu \equiv \xi - U_c\tau \qquad \text{(A2-11)}$$

Next, consider the influence of x, y and z to be small compared to ξ, η and ζ and combine Eqs. (A2-9) and (A2-10).

$$Q_s(\xi,\tau) = -\int_{-\infty}^{\infty}\int_{-\infty}^{\infty} \frac{\partial^2}{\partial \xi^2} Q\,(R,\tau)\,d\eta\,d\xi \qquad \text{(A2-12)}$$

Then it can be shown that

$$\left[\frac{\partial Q}{\partial \xi}\right]_{\eta,\zeta,\tau} = \frac{\partial Q}{\partial R}\frac{\mu}{R} \qquad \text{(A2-13)}$$

$$\left[\frac{\partial^2 Q}{\partial \xi^2}\right]_{\eta,\zeta,\tau} = \frac{1}{R}\frac{\partial Q}{\partial R} + \frac{\mu^2}{R}\frac{\partial}{\partial R}\left[\frac{1}{R}\frac{\partial Q}{\partial R}\right] \qquad \text{(A2-14)}$$

The area integral $\int_{-\infty}^{\infty}\int_{-\infty}^{\infty} d\eta d\zeta$ of Eq. (A2-12) which is the cross sectional area of the jet can be evaluated by the following change of variable:

$$r^2 \equiv \eta^2 + \zeta^2 \tag{A2-15}$$

The integration of r is from 0 to ∞. Thus

$$\int_{-\infty}^{\infty}\int_{-\infty}^{\infty} d\eta d\zeta = 2\pi \int_0^{\infty} r\,dr \tag{A2-16}$$

For integration across the radial plane μ and τ are constant and from Eq. (A2-10) it can be shown that

$$r\,dr = R\,dR \tag{A2-17}$$

The integration of R is from μ to ∞. Therefore Eq. (A2-12) becomes the following after introducing Eqs. (A2-14), (A2-16) and (A2-17):

$$Q_s(\xi,\tau) = -2\pi \int_{\mu}^{\infty} \left\{ \frac{1}{R}\frac{\partial Q}{\partial R} + \frac{\mu^2}{R}\frac{\partial}{\partial R}\frac{1}{R}\frac{\partial Q}{\partial R} \right\} R\,dR \tag{A2-18}$$

By integration Eq. (A2-18) becomes

$$Q_s(\xi,\tau) = 2\pi \frac{\partial}{\partial \mu}\left[\mu\, Q\,(\mu,\tau)\right] \tag{A2-19}$$

After a second integration and noting that $\mu = \xi - U_c\tau$, the desired autocorrelation function Q can be made the dependent variable.

$$Q(\mu,\tau) = \frac{1}{2\pi\mu}\int_{\xi=U_c\tau}^{\xi=\mu+U_c\tau} Q_s(\xi,\tau)\, d\xi \tag{A2-20}$$

Then by applying L'Hospital's Rule to Eq. (A2-20)

$$Q(0,\tau_i) = \frac{1}{2\pi}\left[Q_s(U_c\tau,\tau_i)\right] \tag{A2-21}$$

Thus the inversion has been completed for the condition of isotropy. The quantity Q_s is evaluated from measurements made with the laser beams that project through the flow. These measurements are integrations across the eddies. It can be shown, however, that at any fixed value of time delay τ, the point $\mu = 0$ corresponds to the maximum values of the $Q_s(\xi,\tau)$ vs ξ curves. This is accomplished by a Taylor series expansion and by the requirement of symmetry around $\mu = 0$. It means that the convection velocity U_c, introduced into Q in Eq. (A2-9) can be evaluated experimentally from the $Q_s(\xi,\tau)$ curves. This convection velocity has significance in itself; however, it is also introduced into the relations that characterize the radiated noise.

The quantity which is related to the noise source term in the acoustic equation is the second derivative of $Q(0,\tau_i)$ with respect to time delay τ. The subscript i denotes the values of τ which establish the envelope of the family of cross correlation curves. Thus the noise radiated outside the jet is related to the fluctuating density inside the jet as follows:

$$\Psi_d \propto \left[\frac{\partial U}{\partial y}\right]^2 \left[\frac{\partial^2 Q(0,\tau_i)}{\partial \tau^2}\right] \tag{A2-22}$$

The validity of the assumption of isotropy for the fluctuating density is not known by experiment at the present time; consequently, the possibilities of relaxing this assumption by means of other models are in order.

A2-4 Nonisotropic fluctuations

Consider a more realistic concept, that for which the surfaces formed by constant values of the cross correlations are ellipsoidal (rather than spherical) with the major axis a, oriented along the flow in the

ξ direction. The other two axes b and c, are not necessarily equal. For this case Eq. (A2-9) may be written as

$$Q_s(x,y,z;\xi,\tau) = -\int_{-\infty}^{\infty}\int_{-\infty}^{\infty} \frac{\partial^2}{\partial \xi^2} Q\left(x,y,z;\sqrt{\frac{\left[\xi - U_c\tau\right]^2}{a^2} + \frac{\eta^2}{b^2} + \frac{\zeta^2}{c^2}},\ \tau\right) d\eta d\zeta \qquad \text{(A2-23)}$$

By following the same procedure of inversion as for the isotropic case, Eq. (A2-21) becomes

$$Q(0,\tau_i) = \frac{1}{2\pi}\left[\frac{a^2}{bc}\right]\left[Q_s\left(U_c\tau,\tau_i\right)\right] \qquad \text{(A2-24)}$$

Eq. (A2-24), which applies for ellipsoidal surfaces is the same as the isotropic relation except for the factor $[a^2/bc]$. Hence, it is apparent that this term increases the autocorrelation function because it is likely that the elongation occurs along ξ (or x) in the direction of largest flow expansion of the jet. An experimental evaluation of the factor $[a^2/bc]$ for the fluctuating density has, however, not been accomplished. Therefore, this approach cannot be used in the analysis of the data unless it were merely for comparative purposes with the use of selected values of $[a^2/bc]$. This has not been done, however. When spherical symmetry does not exist, the rotational effect must also be taken into account, however, this effect is not considered here.

A 3 MICROPHONE ANALYSIS

The theory for the evaluation of the autocorrelation function Ψ_n, of the radiated noise as determined from measurements obtained with the use of pairs of microphones is described in detail by Parthasarathy in Ref. 12. There, stationary noise sources are considered first and then the theory is extended to moving sources such as those that occur in subsonic and in supersonic jets. For subsonic jets, as considered in this investigation, the experimentally determined cross correlation function $C(\tau)$, may be expressed as

$$C(\tau) = n\int_{\infty} \frac{\Psi_n\left(t - \tau - \frac{r_1}{a_o}(t-\tau),\ t - \frac{r_2}{a_o}(t)\right) dt}{r_1(t-\tau)\left[1 - M_c\cos\theta_1(t-\tau)\right]^2 r_2(t)\left[1 - M_c\cos\theta_2(t)\right]^2} \qquad \text{(A3-1)}$$

The lower limits of integration are:

$$T_2 \quad \text{if} \quad T_2 > T_1 + \tau$$

$$T_1 + \tau \quad \text{if} \quad T_2 < T_1 + \tau$$

In Eq. (A3-1) the autocorrelation function of the noise Ψ_n, contains the constant $1/16\,\pi^2$. The cross correlation function $C(\tau)$, is evaluated from experimental measurements and the unknown variable is the autocorrelation function of the noise Ψ_n, in the moving frame of reference of the eddies. Thus, in order to evaluate Ψ_n Eq. (A3-1) must be inverted. To do this it is convenient to consider Ψ_n as a function of a time difference $\Delta t = t_2 - t_1$ and t_2. By referring to Eq. (A3-1) it will be noted that if t_2 is set equal to $(t - r_2(t)/a_o)$, then Δt is $(r_2(t)/a_o - r_1(t-\tau)/a_o + \tau)$. It is also convenient to represent Ψ_n in the form

$$n\Psi_n(\Delta t, t_2) = \sum_{i=1}^{N_1} g_i(t_2)\,\phi_i(\Delta t) \qquad \text{(A3-2)}$$

Thus, g_i is a function of t_2 only and ϕ_i is a function of Δt only. The quantity $\phi_i(\Delta t)$ is chosen to be the autocorrelation functions representing the noise in the various octave (or wider) bands N_1. These functions are of the type (Ref. 12):

$$\phi_i(\Delta t) = \cos 2\pi f_i \Delta t\ \frac{\sin\frac{\alpha-1}{\alpha+1}2\pi f_i\Delta t}{\frac{\alpha-1}{\alpha+1}2\pi f_i\Delta t} \qquad \text{(A3-3)}$$

Thus, Eq. (A3-3) represents an autocorrelation function for each chosen band. The frequency f_1, is at the center of this band and the ratio of the highest frequency at the edge of the band to the lowest frequency is α. For an octave band, $\alpha = 2$.

The other function in Eq. (A3-2), $g_1(t_2)$, is taken to be piece-wise linear with value $g_1(j\delta)$ defined at the nodes 0, δ, ---$j\delta$---$N_2\delta$ along t_2. Therefore, in Eq. (A3-2) there are N_1N_2 unknown coefficients that must be determined to evaluate Ψ_n. These coefficients can be determined from a set of simultaneous equations that result from the use of Eq. (A3-1) if known values of the cross correlations and of the autocorrelations are introduced for $C(\tau)$. Evaluation of the unknown coefficients involves the use of inversion by least squares. Only positive values of the coefficients are selected since the noise is being radiated out of the jet. A numerical example of the procedure is given in Section 9, RADIATED NOISE.

NOTATION

a,b,c	ξ, η and ζ axes of ellipsoid respectively Eq. (A2-23)
a_o	speed of sound at ambient conditions
C	cross correlation function
D	diameter of jet at flow separation
e	voltage signal output of laser detector
f	frequency
g	a function of time, Eq. (A3-2)
G	a fluctuating random scalar function
I	noise intensity
ℓ	beam length between edge of jet and knife edge
L	that portion of the laser beam length which lies within the jet diameter (Fig. A2-1)
M	Mach number based on speed of sound at ambient temperature
M_j	jet Mach number based on speed of sound at jet temperature
n	number of sources per unit time which emit sound; also the refractive index
N_1	number of frequency bands
N_2	number of nodal points
p	static pressure
p_t	stagnation pressure
p_w	static pressure at the wall
Q	two-point correlation of the density fluctuations = $\overline{\rho_V' \rho_H'}$
Q_s	experimental cross correlation function of the laser signals
R	defined by Eq. (A2-10); also the distance from the center of the nozzle at the exit to a microphone, Eqs. (2) and (3)
r	distance from noise source to microphone; also a variable defined by Eq. (A2-15)
S	sensitivity of the detector
t,t*	time
T	time required for sound to travel from the nozzle exit (origin of first sound wave) to a microphone, Eq. (A3-1); also temperature
U	mean jet velocity
U_c	convection velocity of the eddies
U_0	mean jet velocity at the nozzle exit or downstream of the normal shock wave
x*	axial distance from flow separation location inside the nozzle
x,y,z	coordinates with the origin at the nozzle exit, see Figs. (A2-1) and (A2-2)
α	ratio of highest frequency at the edge of a band to the lowest frequency of the band, Eq. (A3-3); also a factor in Eqs. (2) and (3)
β	emission angle, the angle between the jet axis and the line joining a microphone with the center of the nozzle at the nozzle exit plane
γ	angular deflection of a laser beam
δ	time increment
ϵ	Gladstone-Dale constant
ζ	coordinate along the z direction with origin on the horizontal laser beam, see Fig. (A2-2)
η	coordinate along the y direction, see Figs. (A2-1) and (A2-2)
θ	angle between the jet axis and a line drawn from a noise source to a microphone
μ	ξ coordinate in moving reference frame, equal to $\xi - U_c\tau$
ξ	coordinate along the x direction, or beam separation distance, see Figs. (A2-1) and (A2-2)
ρ	density
τ	time delay

τ_* time delay for which the rms density fluctuations decay to one-half the maximum value

φ autocorrelation functions representing the noise in the various frequency bands, Eq. (A3-3)

Ψ autocorrelation function in moving frame of reference of the eddies

( ) denotes "function of"

[ ] or $\{ \}$ denotes "multiplied by"

< > denotes averages

$\_$ denotes a vector quantity when it appears beneath a symbol

SUBSCRIPTS

a ambient conditions inside the anechoic chamber

c convection of eddies

d density

e emission conditions

H horizontal beam

i index

n noise

q quadrupole

t stagnation condition

V vertical beam

β at angle β with respect to the jet axis

ζ along the ζ direction

η along the η direction

ξ along the ξ direction

0 initial condition; also nozzle inlet condition

1,2 microphone numbers; also different times or locations; also indexes

78,90 78° and 90° with respect to the jet axis

SUPERSCRIPTS

' fluctuating quantity (indicated in figures but not in equations)

$\bar{}$ average value

NASA — JPL — Coml., L.A., Calif.